INTERNATIONAL JOURNAL FOR NUMERICAL METHODS IN FLUIDS, VOL. 16, 683–696 (1993)

NUMERICAL SIMULATION OF AN ISOLATED VORTEX AND SHEAR FLOW INTERACTION

I. V. ANTROPOV

Vernadsky Institute of Geochemistry and Analytical Chemistry, Moscow, Russia

SUMMARY

A numerical solution for the Navier–Stokes equations in the unbounded region is considered for the interaction of an isolated vortex and shear flow. A Chebyshev collocation method in space and finite-difference method for temporal discretization are used. The results of the numerical experiments for the interaction are discussed. It is shown that shear flow can both increase and decrease the vortex dissipation rate.

KEY WORDS Collocation Incompressible flow Shear layer Unbounded region Vortex

INTRODUCTION

Vortex evolution processes are inherent in many naturally occurring phenomena, both large scale (atmospheric cyclones) and small scale (the turbulization of a shear flow). It has long been observed that the free shear layer contains large-scale spanwise vortices at a wide variety of Reynolds numbers. There have been numerous studies of the formation, stability, evolution and interactions of these vortices. Waugh and Dritshel[1] investigated the stability of filamentary vorticity for a class of two-dimensional, inviscid, non-divergent models. In all models, a strip of potential vorticity is unstable in the absence of background shear flow. Imposing a shear flow that reverses the total shear across the strip, however, brings about stability. On the other hand, although co-operative shear can suppress linear instability, it cannot prevent non-linear disruption. Metcalfe *et al.*[2] investigated three-dimensional stability of two-dimensional vortical states by direct numerical solution of Navier–Stokes equations. Three-dimensional computations with random initial conditions were performed by Sandham and Reynolds,[3] who investigated the influence of compressibility on the development of large-scale structures. Both Metcalfe *et al.*[2] and Sandham and Reynolds[3] assumed periodicity of the flow in two directions. A Fourier collocation method for these directions was used. For the third direction, Chebyshev collocation method was used by Metcalfe *et al.*[2] and finite-difference method by Sandham and Reynolds.[3] Marcus[4] considered two-dimensional, inviscid, constant-density, quasi-geostrophic flow between rapidly rotating annuli. He showed that the dynamics depends crucially on the exchange between the self-energy of the flow and the interaction energy of the zonal flow with the vortices. The Fourier–Chebyshev collocation method was used for numerical computations. Experimental investigations of a plane shear layer and the vortex dynamics in it have been made by Lasheras *et*

* Address correspondence to Mr. I. V. Antropov at Universitetsky prospekt 4-11, Moscow, Russia.

0271–2091/93/080683–14$12.00

Received February 1992
Revised November 1992

al.,[5] Lasheras and Cho,[6] Bernal and Roshko,[7] Nygaard and Glezer[8] and Panides and Chevray.[9]

In this work we consider two-dimensional, viscid, constant-density, incompressible flow in Cartesian co-ordinates. The paper seeks to describe an isolated vortex and shear flow interaction process using Chebyshev collocation method for space co-ordinates and high-accuracy finite-difference scheme for time discretization. The outline of the paper is as follows. First, the numerical procedure is considered. Next, the isolated vortex is simulated using the numerical procedure. Here the objective is twofold: to compare numerical simulation results with analytical solution for isolated vortex, and to choose proper time step and iterative parameters. After that, the results of the simulation of the isolated vortex and shear flow interaction are shown. Finally, the possibilities of an algorithm generalization for inhomogeneous and three-dimensional flows are briefly discussed.

NUMERICAL SOLUTION PROCEDURE

The collocation (pseudo-spectral) method is one of the spectral methods. It has the advantage of a high degree of accuracy of the spectral methods, as well as the possibility of dealing with non-linear terms of differential equations in physical space. For a complete discussion of spectral methods application to partial differential equations numerical integration, the reader is referred to Gottlieb and Orszag,[10] Canuto *et al.*[11] and references therein.

The computer procedure used for numerical simulations considered in this article is developed as follows: Denote velocity as $V=(u, v)$, time as t, space co-ordinates as x and y, pressure as P, Reynolds number as Re. All variables here and below are assumed to be dimensionless. The Navier–Stokes equations in Cartesian co-ordinates are

$$\frac{\partial V}{\partial t}+\nabla\cdot(VV)=\frac{1}{Re}\Delta V-\nabla P \tag{1}$$

and the incompressible fluid continuity equation is

$$\nabla\cdot V=0. \tag{2}$$

Let us transform the (x, y) plane to the square $[-1, 1]\times[-1, 1]$: $\bar{x}=\tanh(x/M)$, $\bar{y}=\tanh(y/M)$ and $M=$constant. For the numerical simulation results shown herein, we set $M=5{\cdot}07$.

Approximation in space

Derivatives of a function $f(x, y, t)$ with respect to x are

$$\frac{\partial f}{\partial x}=S\frac{\partial f}{\partial \bar{x}}\quad \frac{\partial^2 f}{\partial x^2}=-\frac{2\bar{x}S}{M}\frac{\partial f}{\partial \bar{x}}+S^2\frac{\partial^2 f}{\partial \bar{x}^2}$$
$$S=\frac{1}{M}\operatorname{sech}^2\left(\frac{1}{2}\ln\frac{1+\bar{x}}{1-\bar{x}}\right). \tag{3}$$

Let us expand $f(\bar{x}, \bar{y}, t)$ with fixed $\bar{y}$ and t in terms of Chebyshev polynomials $T_k(\bar{x})$:

$$f(\bar{x})=\sum_{k=0}^{\infty}\hat{f}_k T_k(\bar{x}).$$

The expansion coefficients are given by

$$\hat{f}_k=\frac{2}{\pi c_k}\int_{-1}^{1} f(\bar{x})T_k(\bar{x})(1-\bar{x}^2)^{-1/2}\,d\bar{x},\quad c_0=2,\ c_k=1\ (k>0). \tag{4}$$

Let us consider the collocation points $\bar{x}_j=\cos(\pi j/N)$, $0\le j\le N$. Denote $f(\bar{x}_j)$ as f_j. The integrals (4) can be substituted with corresponding sums

$$\hat{f}_k=\frac{2}{N\bar{c}_k}\sum_{j=0}^{N}\frac{1}{\bar{c}_j}f_j\cos\frac{\pi jk}{N},\quad 0\le k\le N,$$
$$\bar{c}_j=\begin{cases}2, & j=0, N,\\ 1, & 1\le j\le N-1.\end{cases}\tag{5}$$

The function values at the collocation points can be written as

$$f_j=\sum_{k=0}^{N}\hat{f}_k\cos\frac{\pi jk}{N},\quad 0\le j\le N.\tag{6}$$

It is shown in Gottlieb and Orszag[10] that, if $f(\bar{x})$ is piecewise continuous and if $f(\bar{x})$ is of bounded total variation for $-1\le\bar{x}\le 1$, then, as N goes to ∞, the expansion (6) converges to $[f(\bar{x}_-)+f(\bar{x}_+)]/2$. Also, if $f^{(p)}(\bar{x})$ is continuous for all $|x|\le 1$ for $p=0, 1, \ldots, N-1$, and $f^{(N)}(\bar{x})$ is integrable, then the error in the Chebyshev series goes to zero more rapidly than any finite power of $1/N$ as N goes to ∞. It follows from the Chebyshev polynomial property that $T_k(\cos\theta)=\cos k\theta$.

If $N=2^m3^n$ (m, n—integer numbers), the sums (5) and (6) can be calculated using the fast Fourier transform. Fast-Fourier-transform-based algorithms provide an efficient way for transition from physical space $\{f_j\}$ to transform space $\{\hat{f}_k\}$ and back to physical space again. Let us expand $\bar{x}$ derivative of $f(\bar{x})$ in terms of Chebyshev polynomials,

$$\frac{\mathrm{d}}{\mathrm{d}\bar{x}}f(\bar{x})=\sum_{k=0}^{\infty}\hat{f}_k^{(1)}T_k(\bar{x}).$$

The coefficients $\hat{f}_k^{(1)}$ can be quickly calculated in $\{\hat{f}_k\}$ using the recurrence relation,

$$c_k\hat{f}_k^{(1)}=\hat{f}_{k+2}^{(1)}+2(k+1)\hat{f}_{k+1},\quad k\ge 0.\tag{7}$$

To calculate advection terms of the Navier–Stokes equations, it is necessary to multiply two functions. Preferably, it should be done in physical space $\{f_j\}$, because the operation of multiplication in $\{\hat{f}_k\}$ is equivalent to sums multiplication. As a rule, initial velocity and pressure fields are defined in physical space. In most cases, boundary conditions are also easier to impose for a function in $\{f_j\}$. These are the reasons to integrate equations (1) and (2) in physical rather than in transform space and to use the transform space only for the evaluation of derivatives.

In the numerical procedure presented herein, the derivatives with respect to the x co-ordinate at collocation points are calculated using expressions (3), (5)–(7). The y-derivatives are calculated in similar fashion. For the results of numerical simulations shown below, N is equal to 32; 33 terms in a sum are retained and a 33×33 grid of collocation points is used.

Approximation in time

The integration of equations (1) and (2) for time is performed as follows. Let $V(t_n)$ denote a velocity field at time step n. At the first half of the time step, the intermediate velocity field V^* is determined as a solution of the equations

$$\frac{\partial V}{\partial t}+\nabla\cdot(VV)=\frac{1}{Re}\Delta V.$$

The finite-difference algorithm is used for time approximation. It combines two schemes. The explicit third-order compact Runge–Kutta scheme suggested by Williamson[12] is used for advection terms $A(V)=-\nabla\cdot(VV)$; the implicit second-order Crank–Nicolson scheme is used for diffusion terms $D(V)=\Delta V/Re$. All derivatives with respect to space variables x and y in $A(V)$ and $D(V)$ are calculated using the collocation method. The intermediate velocity field V^* is determined as follows ($\tau=\Delta t/2$, half of the time step):

$$\begin{aligned} V_0&=V(t_n),\\ H_1&=\tau A(V_0),\\ V_1&=V_0+\tfrac{1}{3}H_1+\tfrac{1}{6}\tau[D(V_0)+D(V_1)],\\ H_2&=\tau A(V_1)-\tfrac{5}{9}H_1,\\ V_2&=V_1+\tfrac{15}{16}H_2+\tfrac{5}{24}\tau[D(V_1)+D(V_2)],\\ H_3&=\tau A(V_2)-\tfrac{153}{128}H_2,\\ V_3&=V_2+\tfrac{8}{15}H_3+\tfrac{1}{8}\tau[D(V_2)+D(V_3)],\\ V^*&=V_3. \end{aligned} \tag{8}$$

Next, the pressure field $P(t_{n+1})$ is calculated as a solution of the Poisson equation,

$$\Delta P=\nabla V^*/\tau.$$

At the second half of the time step, the velocity field is corrected in order to insure mass conservation for $V(t_{n+1})$:

$$V(t_{n+1})=V^*-\tau\nabla P(t_{n+1}).$$

The numerical procedure described above was used successfully by Street and Hussaini[13] for numerical simulation of Taylor–Couette flow in cylindrical co-ordinates. Two Helmholtz equations are solved for $V_i=(u_i, v_i)$, $i=1, 2, 3$. Thus, the algorithm realization requires solution of six Helmholtz equations for the intermediate velocity field evaluation and one Poisson equation for pressure at each time step. To solve these equations, the minimal residual method is used.

Let us write $Lf=b$ for each of the Helmholtz and Poisson equations, where f is the function to be found, and b is the right-hand side of the equation. With R_k to denote the residual at the iteration k, we have $R_0=b-Lf_0$, $R_{k+1}=R_k-\alpha_k LR_k$; the solution approximation at $k+1$ iteration is defined as $f_{k+1}=f_k+\alpha_k R_k$. The iteration parameter α_k is chosen in order to minimize the squared norm of R_{k+1} in L_2 space:

$$(R_{k+1}, R_{k+1})=(R_k, R_k)+\alpha_k^2(LR_k, LR_k)-2\alpha_k(R_k, LR_k).$$

Equating the derivative of this expression with respect to α_k to zero, the optimal α_k value can be derived: $\alpha_k=(R_k, LR_k)/(LR_k, LR_k)$. Obviously, with this choice of α_k, the squared residual norm is decreasing at each iteration:

$$(R_{k+1}, R_{k+1})=(R_k, R_k)-(R_k, LR_k)^2/(LR_k, LR_k).$$

When it becomes less than the predetermined parameter ε, the iterative cycle is terminated. Unfortunately, the convergence rate of this method deteriorates abruptly when it is applied to the Neumann problem. The convergence rate deterioration for minimal residual and orthogonal residual methods has also been observed by Street and Hussaini.[13] In this work we consider Dirichlet boundary conditions only.

The above numerical procedure can be used for simulations of viscous incompressible fluid

flows. In this work it is implemented to simulate an interaction of an isolated vortex and a shear flow in an unbounded region.

ISOLATED VORTEX SIMULATIONS

Let us consider the situation when, at the moment $t=0$, the infinite length vorticity filament of intensity Γ is placed into an unbounded three-dimensional region. It is called an isolated vortex. We denote the radial distance on the (x, y) plane perpendicular to the vortex axis as r; $r=(x^2+y^2)^{1/2}$. It is shown in Loytsiansky[14] that the vorticity for $t>0$ is distributed as follows:

$$\Omega(x, y, t)=\frac{Re\Gamma}{4\pi t}\exp\left(-\frac{Re\, r^2}{4t}\right). \tag{9}$$

With $U(x, y, t)=(\Gamma/2\pi r)\,[1-\exp(-Re\, r^2/4t)]$, the velocity field corresponding to the vorticity field is

$$u=Uy/r, \qquad v=-Ux/r. \tag{10}$$

The time step may be denoted as Δt, the maximal velocity as $V_{\max}$, and the minimal distance between the collocation points as $\Delta x_{\min}$. The finite-difference scheme used for integration for time is stable for a Courant number, $C=\Delta t\, V_{\max}/\Delta x_{\min}$, up to one. However, for most time-dependent problems, the error value due to time discretization is more important for the choice of the time step Δt than the scheme stability. The time step in Street and Hussaini[13] was chosen so that the Courant number was about 0·1–0·2.

To choose the time-step value and values of squared residual norm ε_v and ε_p used for termination of iterations for solving of Helmholtz and Poisson equations, a numerical simulation of isolated vortex dissipation was carried out. Several runs with $\Gamma=10$, $Re=10$ and $2\leq t\leq 12$ were performed. The initial velocity field was calculated using equation (10) for $t=2$. The plot of

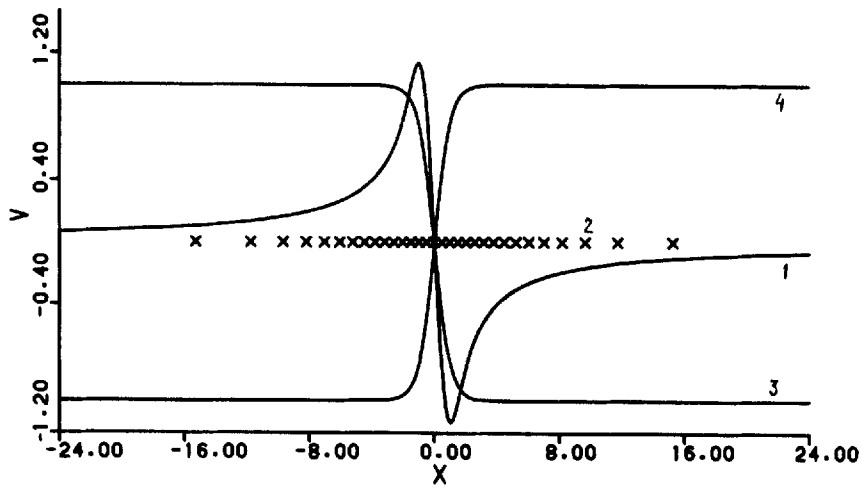

Figure 1. The distribution of the velocity y-component v and collocation points on the x-axis: (1) the distribution of isolated vortex velocity y-component $v(x, 0)$ at $t=2$; (2) collocation points distribution ($M=5{\cdot}07$, $N=32$); (3) shear flow velocity y-component distribution $v(x)$ in the case when the sense of shear is coincident with the sense of the vortex rotation; (4) shear flow velocity y-component distribution $v(x)$ in the case when the sense of shear is opposite to the sense of the vortex rotation

v as a function of x for $y=0$ and $t=2$ and the distribution of collocation points along the x-axis are shown in Figure 1. The boundary collocation points (first and 33rd) are located at $\pm\infty$. The values ε_v, ε_p and Δt had been decreased with each subsequent run until velocity and pressure fields ceased to differ from the fields at the same time moments for the previous run. For the numerical simulations discussed below, the time step $\Delta t=5\times10^{-3}$ has been chosen ($C=6{\cdot}5\times10^{-3}$), although the numerical scheme remains stable for a much larger time step. In fact, with Δt chosen so small, the error because of time discretization can be neglected, and we have to deal with the error in advection and diffusion terms only. With these ε_v, ε_p values and Δt, only 1–2 iterations for every variable at each time step are sufficient. Several time steps in the beginning are exceptions. A maximum number of iterations (600–700) is necessary for solving the Poisson equation for pressure at the first time step, because $P(x, y)=0$ is used as an initial approximation. In other cases, either the field at the previous time step or intermediate velocity fields (V_1 for the evaluation of V_2, V_2 for the evaluation of V_3; see equations (8)) were used.

To compare numerical simulation results with an analytical solution vorticity field, $\Omega(x, y)=(\partial u/\partial y)-(\partial v/\partial x)$ was calculated every 10th time step. The x and y derivatives were estimated using equations (3), (5)–(7). The vorticity plots for $-15{\cdot}28\leq x, y\leq 15{\cdot}28$, $t=2$ and $t=12$ are shown in Figure 2. The vorticity field for the initial approximation is shown in Figure 2(a). We denote the maximal vorticity value as $\Omega_{\max}$; $\Omega_{\max}=\Omega(0, 0)=4{\cdot}01$. The maximum difference between the analytical solution (9) and the vorticity approximation with space derivatives estimated using the collocation method is equal to $3{\cdot}4\times10^{-2}$ (at $x=1$, $y=1$ point). When equations (1) and (2) are integrated with the initial approximation and Dirichlet boundary conditions ($u|_{r=\infty}=0$, $v|_{r=\infty}=0$, $P|_{r=\infty}=0$), the difference between numerical and analytical solutions grows initially and then begins to decrease with vortex dissipation. The maximum difference for vorticity approaches 0·71 at $t=4{\cdot}90$, $x=0$, $y=0$, which is 18 per cent of $\Omega_{\max}$. The vorticity field at $t=12$ (after 2000 time steps) is shown in Figure 2(b). The maximum difference between numerical and analytical solutions is equal to 0·52 (13 per cent of $\Omega_{\max}$) at the origin ($x=0$, $y=0$).

Thus, analytical and numerical solutions at the origin differ noticeably. The usual spectral accuracy cannot be achieved in this example because the numerically simulated $P(x, y)$ is different from the pressure field corresponding to (9). The numerical solution is the sum of bounded variation functions; it has a finite value for any x and y. On the other hand, for analytical solution $\lim_{r\to 0}(P)=-\infty$ (with the boundary condition $P|_{r=\infty}=0$). It is for this reason that the analytically calculated vortex dissipates faster than the numerically simulated one. The difference between numerical and analytical solutions decreases slightly with collocation points moving closer to the origin (M decreasing) and increases as they move apart (M increasing). The attempt to improve accuracy by moving collocation points closer to the origin entails the development of small-scale oscillations in the simulations of isolated vortex and shear flow interaction considered below. Therefore, the choice of M equal to 5·07 is, in a sense, a compromise to achieve satisfactory grid resolution for the whole of the region of interest. Since the behaviour of the numerically simulated vortex and the analytically calculated one is qualitatively the same, it is still possible to apply the above algorithm to the simulation of interaction between an isolated vortex and a shear flow. The aim of the discussion to follow is to describe the main features of this interaction.

INTERACTION SIMULATIONS

Let us consider a shear flow with initial velocity field

$$u(x, y)=0, \qquad v(x, y)=\pm\tanh(x). \tag{11}$$

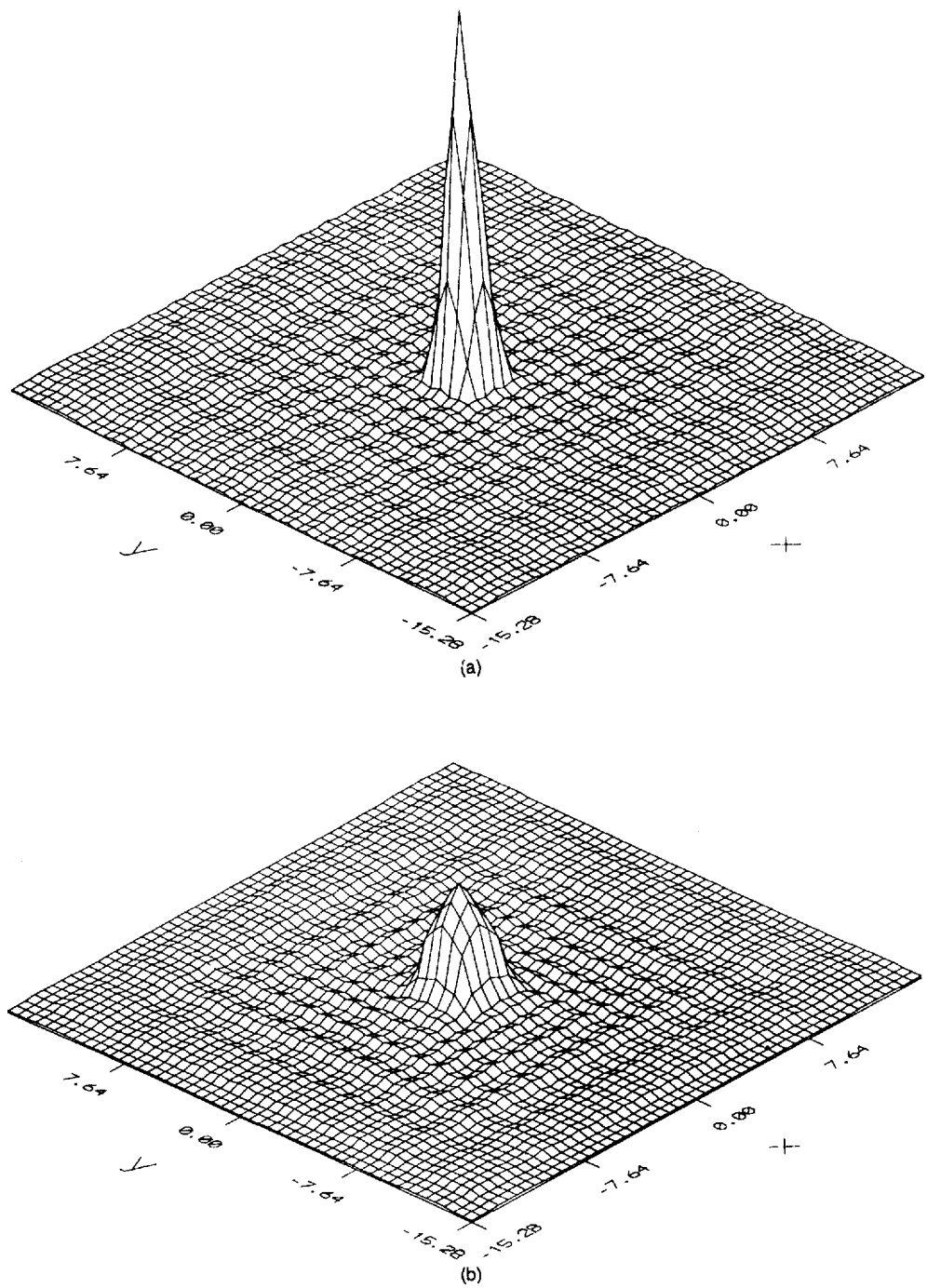

Figure 2. The distributions of the vorticity $\Omega(x, y)$.
(a) $t=2$, (b) $t=12$ isolated vortex simulation.
(c) $t=2$, (d) $t=12$ isolated vortex and shear flow interaction; the sense of shear is coincident with the sense of the vortex rotation.
(e) $t=2$, (f) $t=12$ isolated vortex and shear flow interaction; the sense of shear is opposite to the sense of the vortex rotation

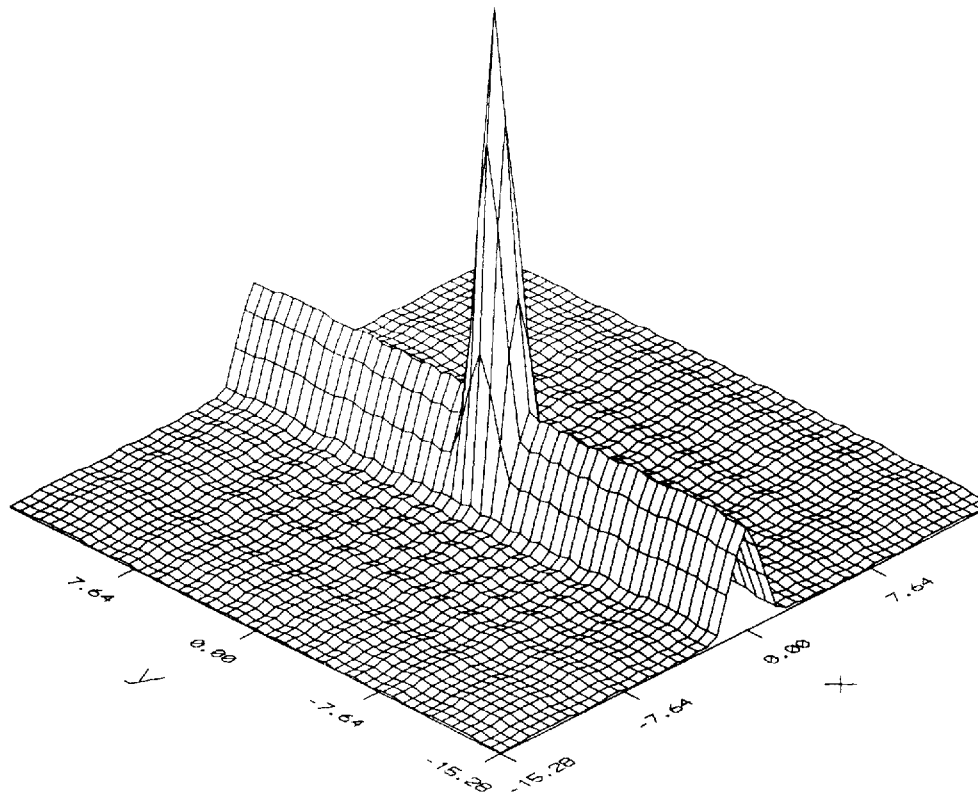

(c)

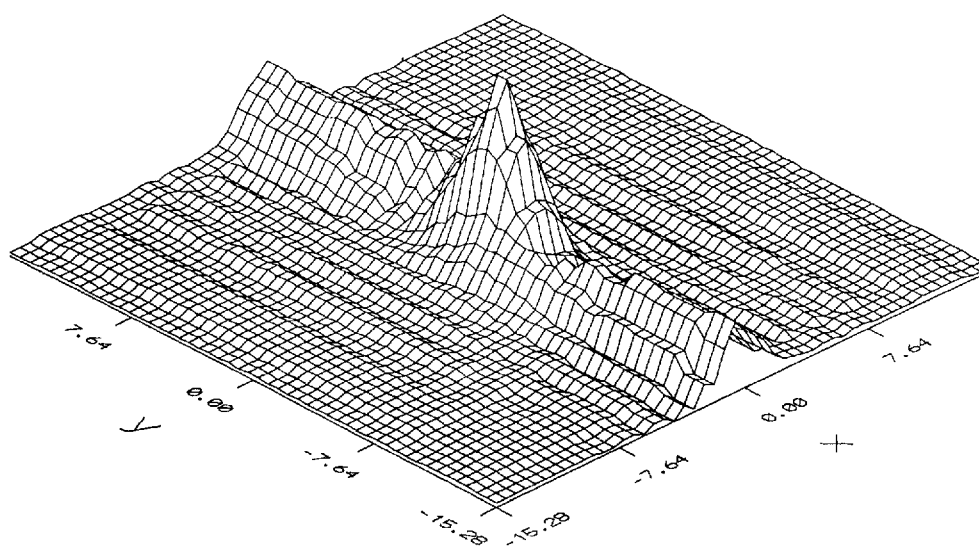

(d)

Figure 2. (Continued)

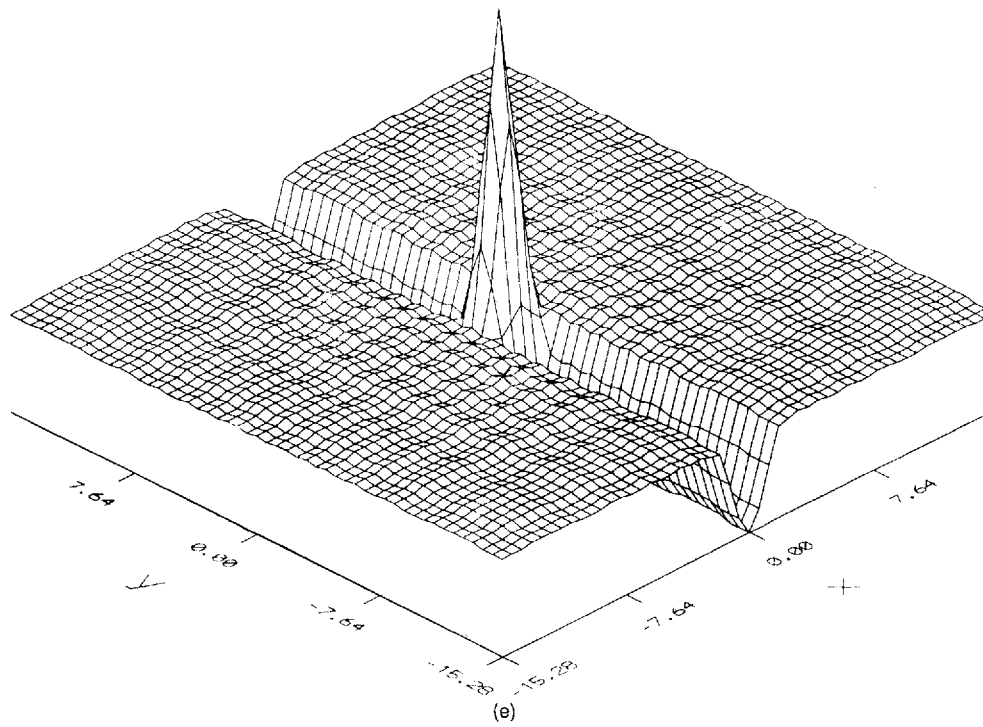

(e)

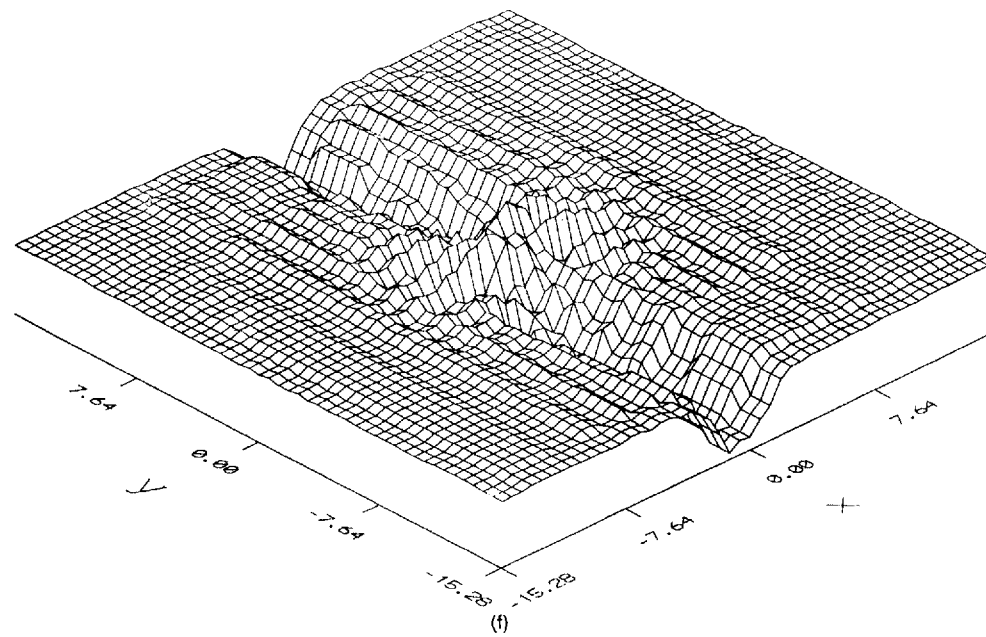

(f)

Figure 2. (Continued)

The sign of the velocity component v corresponds to shear sense (direction). Two alternate interaction variants corresponding to different shear directions will be discussed below. The shear flow vorticity field is

$$\Omega(x, y) = \pm \operatorname{sech}^2 x. \tag{12}$$

We use, for initial approximation, the superposition of the velocity fields calculated with equation (10) for $t = 2$ and equation (11). The initial shear flow velocity distributions are shown in Figure 1, where curve 3 corresponds to the case when negative signs in equations (11) and (12) are used. Assuming a clockwise rotating vortex, the sense of rotation of the vortex is coincident with the sense of shear. The curve 4 corresponds to the case when positive signs in (11) and (12) are used; the sense of the vortex rotation is opposite to the sense of shear. The initial vorticity fields are the superposition of the fields calculated by (9) and (12) and are shown in the Figures 2(c) and 2(e). The vorticity fields for these plots were approximated using the initial velocity fields; the x- and y- derivatives were calculated using the collocation method. The differences between these vorticity distributions and those calculated with (9) and (12) ones are maximal at the points with $x = 0$, $y = \pm 1.28$ co-ordinates; their values are insignificant (about 10^{-2}).

Let us consider the boundary conditions imposed at infinity in more detail. With $Re < \infty$, the velocity field (11) is not the solution of equations (1) and (2) for any t. In other words, the usage of the distribution (11) as an initial approximation gives rise to a time-dependent flow, which tends to change the v profile to a linear one. However, the shear flow simulation performed for $Re = 10$, with velocity distribution (11) and $P = 0$ used as boundary conditions at infinity has shown that the velocity field changes for $0 \leq t \leq 10$ are insignificant. Therefore, viscosity effects can be neglected for pure shear flow for this time interval, and one can regard this flow as time-independent. Thus, it is possible to use the velocity distribution (11) and $P = 0$ as boundary conditions at infinity for the isolated vortex and shear flow interaction simulations.

The vorticity fields for $t = 12$ are shown in Figures 2(d) and 2(f). Figure 2(d) corresponds to the case when the sense of rotation of the vortex is coincident with the sense of shear, while Figure 2(f) corresponds to the case when they are opposite to each other. The contour lines corresponding to the Figures 2(d) and 2(f) vorticity distributions are shown in Figure 3. We compare Figure 2(d) with 2(f) and Figure 3(a) with 3(b). As can be seen, shear flow accelerates dissipation of the vortex in the first case, and slows it in the second case. To prove this conclusion, we plot the x-component of the velocity u at the two points on the y-axis as a function of time. This velocity component can be called the tangential velocity. The functions $u(t)$ for the points $x = 0$, $y = 1$ and $x = 0$, $y = 2$ are shown in Figure 4. The points (0, 1) and (0, 2) are marked in Figures 3(a) and 3(b). Three curves are plotted for each point: the curve for vortex flow in the absence of shear and the curves for two flows with alternate shear senses. The x-components of the velocities at the considered points are the same initially (for $t = 2$), because for the pure shear flow, $u = 0$. For $t > 2$, tangential velocities for these three cases at the two points begin to differ.

When the sense of shear coincides with the sense of rotation (curves 1 in Figures 4(a) and 4(b), the tangential velocity at the end of the run exceeds the tangential velocity for the simulation of isolated vortex in absence of shear flow (curves 2 in Figures 4(a) and 4(b)). Note that tangential velocity at the point (0, 2) grows in this case in the beginning of the run (curve 1 in Figure 4(b)). When the sense of shear is opposite to the sense of vortex rotation (curves 3 in Figures 4(a) and 4(b)), the tangential velocity at the considered points is lower than the tangential velocity for an isolated vortex in the absence of shear and decreases monotonically. Thus, shear flow can both increase and decrease the vortex dissipation rate. Similar results are reported by Marcus[4] for inviscid fluid beween rotating annuli. He points out that if the shear and the vortex strength are of the same order and opposite sign, the vortex is pulled into a thin spiral, fragments and is

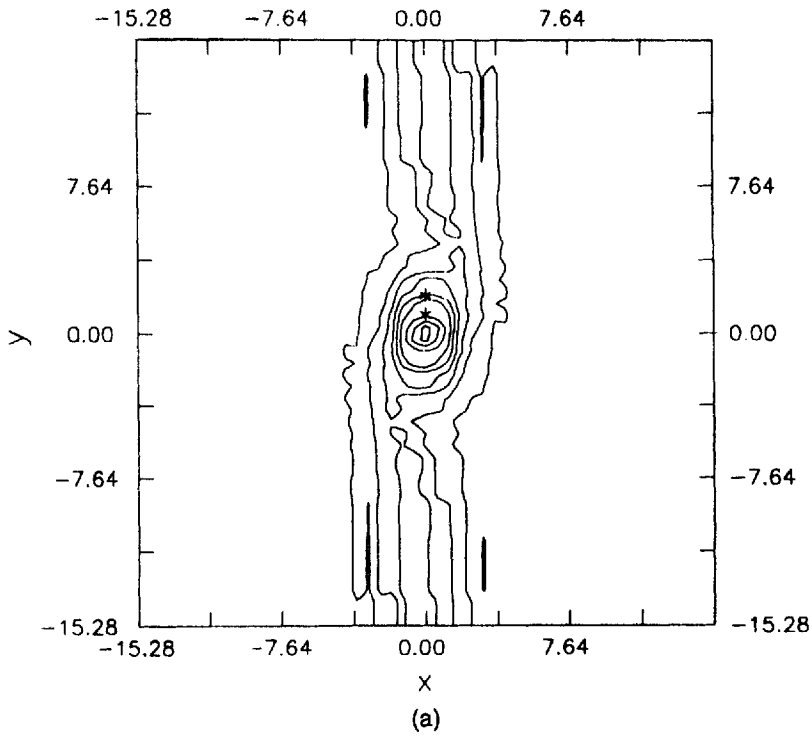

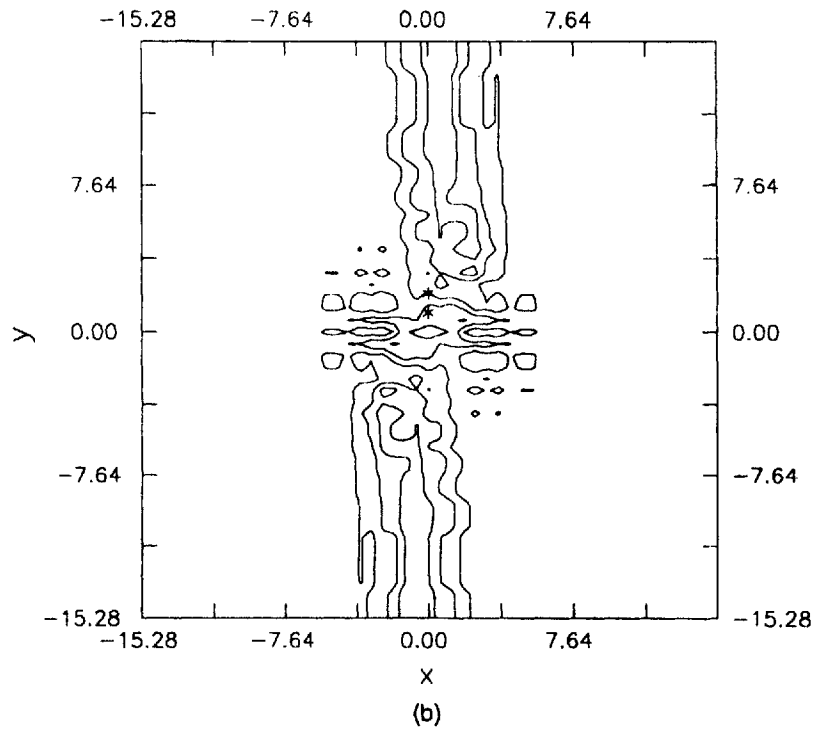

Figure 3. The vorticity $\Omega(x, y)$ contour lines at $t=12$: (a) the sense of shear is coincident with the sense of the vortex rotation; (b) the sense of shear is opposite to the sense of the vortex rotation

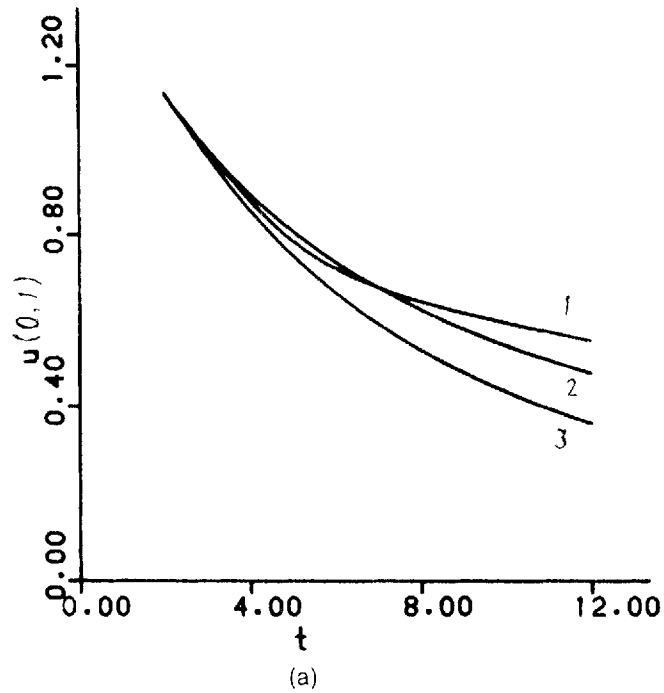

(a)

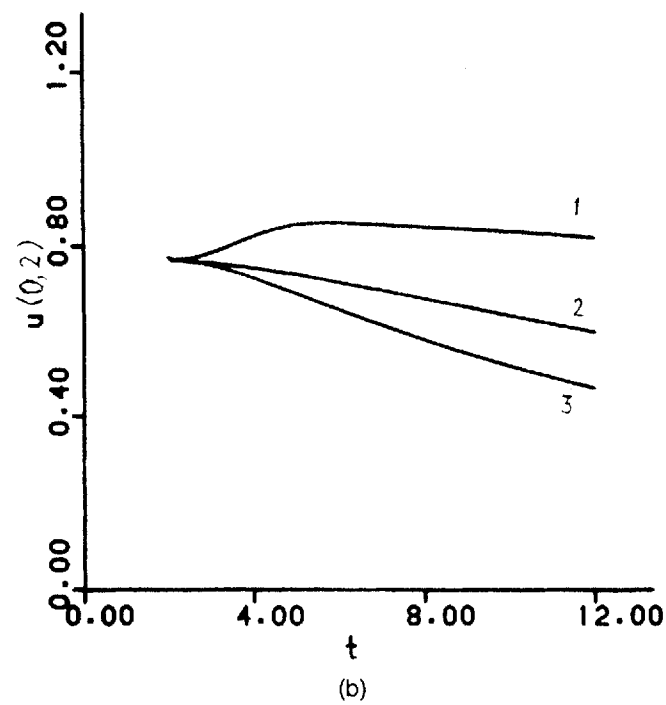

(b)

Figure 4. The velocity x-component u as a function of time t: (1) the sense of shear is coincident with the sense of the vortex rotation; (2) isolated vortex in the absence of shear; (3) the sense of shear is opposite to the the sense of the vortex rotation. (a) $x=0$, $y=1$; (b) $x=0$, $y=2$

destroyed. If the signs are the same, the vortex redistributes its vorticity, and its shape is determined by the ratio of its vorticity to the shear of the surrounding zonal flow.

We next focus our attention on the sense of the Reynolds number introduced above. Normally, Reynolds number for a shear flow is based on the velocity difference $\Delta v = v_1 - v_2$ and on the shear flow thickness. However, it is hard to define the shear flow thickness distinctly. Bernal and Roshko[7] determined it as a visual thickness of a shear layer for a gas facility and as a vorticity thickness for a water facility used in their experiments. The Reynolds numbers ranged from 9400 to 13 300 for the gas facility, and from 1900 to 6500 for the water facility. Lasheras *et al.*[5] estimated local Reynolds numbers based on overall momentum thickness of a shear layer. The Reynolds numbers in their water facility experiments varied from 36 near the trailing edge of the splitter plate to 270 at 25 cm downstream. Nygaard and Glezer[8] also measured momentum thickness of a shear layer. Momentum-thickness-based local Reynolds numbers for their water facility varied from 216 to 1450.

Momentum thickness of a shear layer is

$$\theta = \frac{1}{(\Delta v)^2} \int_{-\infty}^{+\infty} [v(x) - v_2]\,[v_1 - v(x)]\,\mathrm{d}x.$$

For the shear flow considered herein, $v(x) = \tanh(x)$, $v_1 = 1$, $v_2 = -1$ and the momentum thickness $\theta = 0.5$. The momentum-thickness-based Reynolds number $Re = 10$. The shear layer thickness can be defined as a vorticity thickness

$$\delta = \Delta v \Big/ \max \left| \frac{\partial v}{\partial x} \right|.$$

In this case, the vorticity-thickness-based Reynolds number $Re_v = 40$. Although the numerical simulation Reynolds numbers Re and Re_v are considerably lower than the local Reynolds numbers for the experimental works, vorticity distribution for the case when the sense of shear coincides with the sense of vortex rotation is similar to side-view visualization photographs of plane shear layers for water facility experiments shown in References 5–8.

CONCLUSIONS

In this paper, we consider a Chebyshev-collocation-based method for unbounded flows. The main features of isolated vortex and shear flow interactions are investigated using this method. The numerical simulation results are similar to those obtained by Marcus[4] for a vortex in a shearing zonal flow. It is worth mentioning that placing of the vortex into higher-strength shear flow gives rise to the propagation of the disturbance up and down in the y direction and to the flow turbulization. Therefore, the results of this paper are applicable to moderate-strength shear flows only.

To conclude the article, we discuss the possibilities of algorithm generalization. For heat convection flow simulations, equations (1) and (2) should be slightly changed and equations for temperature and density should be considered. If boundary conditions at infinity are defined for all variables, these changes would not cause much difficulty. The numerical procedure described above can be used also for a three-dimensional problem solution. In this case, nine Helmholtz equations should be solved at the first half of time step. The computer code used for the numerical simulations presented in this article is written for three-dimensional case. It is adapted for two-dimensional problem solution with the exclusion of some of the program modules. However, to obtain adequate results in reasonable time for a three-dimensional problem, one would have to use a more powerful computer than the MicroVAX-II computer used for the simulations presented above.

REFERENCES

1. D. W. Waugh and D. G. Dritshel, 'The stability of filamentary vorticity in two-dimensional geophysical vortex-dynamics models', *J. Fluid Mech.*, **231,** 575–598 (1991).
2. R. W. Metcalfe, S. A. Orszag, M. E. Brachet, S. Menon and J. J. Riley, 'Secondary instability of a temporary growing mixing layer', *J. Fluid Mech.*, **184,** 207–243 (1987).
3. N. D. Sandham and W. C. Reynolds, 'Three-dimensional simulations of large eddies in the compressible mixing layer', *J. Fluid Mech.*, **224,** 133–158 (1991).
4. P. S. Marcus, 'Vortex dynamics in a shearing zonal flow', *J. Fluid Mech.*, **215,** 393–430 (1990).
5. J. C. Lasheras, H. Cho and T. Maxworthy, 'On the origin and evolution of streamwise vortical structures in a plane free shear layer', *J. Fluid Mech.*, **172,** 231–258 (1986).
6. J. C. Lasheras and H. Cho, 'Three-dimensional instability of a plane shear layer: an experimental study of the formation and evolution of streamwise vortices', *J. Fluid Mech.*, **189,** 53–86 (1988).
7. L. P. Bernal and A. Roshko, 'Streamwise vortex structure in plane mixing layers', *J. Fluid Mech.*, **170,** 499–525 (1986).
8. K. J. Nygaard and A. Glezer, 'Evolution of streamwise vortices and generation of small scale motion in a plane mixing layer', *J. Fluid Mech.*, **231,** 257–301 (1991).
9. E. Pandies and R. Chevray, 'Vortex dynamics in a plane, moderate Reynolds number shear layer', *J. Fluid Mech.*, **214,** 411–436 (1990).
10. D. Gottlieb and S. A. Orszag, *Numerical Analysis of Spectral Methods: Theory and Applications*, SIAM-CBMS, Philadelphia, 1977.
11. C. Canuto, A. Quarteroni, M. Y. Hussaini and T. A. Zang, *Spectral Methods in Fluid Dynamics*, Springer, New York, 1988.
12. J. H. Williamson, 'Low-storage Runge–Kutta schemes', *J. Comput. Phys.*, **35,** 48–55 (1980).
13. C. L. Street and M. Y. Hussaini, 'Finite length Taylor–Couette flow', in D. L. Dwoyer, M. Y. Hussaini (eds), *The Stability of Time-Dependent Spatially Varying Flows*, Springer, New York, 1987, pp. 312–334.
14. L. G. Loytsiansky, *Fluid and Gas Mechanics* (In Russian), Nauka, Moscow, 1987.